Porous Organic Polymer Films with Tunable Work Functions and Selective Hole and Electron Flows for Energy Conversions

Cheng Gu+, Ning Huang+, Youchun Chen+, Huanhuan Zhang, Shitong Zhang, Fenghong Li, Yuguang Ma, and Donglin Jiang*

Abstract: *Organic optoelectronics are promising technologies for energy conversion. However, the electrode interlayer, a key material between active layers and conducting electrodes that controls the transport of charge carriers in and out of devices, is still a chemical challenge. Herein, we report a class of porous organic polymers with tunable work function as hole- and electron-selective electrode interlayers. The network with organoborane and carbazole units exhibits extremely low work-function-selective electron flow; while upon ionic ligation and electro-oxidation, the network significantly increases the work function and turns into hole conduction. We demonstrate their outstanding functions as anode and cathode interlayers in energy-converting solar cells and light-emitting diodes.*

Organic energy-converting devices possess great economic potential and have a promising future in leading to a new generation of consumer devices that combine low cost, lightweight, and mechanical flexibility.[1] However, the electrode interlayer, a key material that determines not only the charge carrier flow but also the device performance, remains a substantial challenge.[1c] An electron-transporting interlayer should have a sufficiently low work function for either the injection of electrons into, or the collection of electrons from, the lowest occupied molecular orbital (LUMO) of active materials. In contrast, a hole-transporting interlayer should

have a high enough work function for the injection of holes into, or the collection of hole from, the highest occupied molecular orbital (HOMO) of active layers. Therefore, electrode interlayers require the design of work function into extreme levels that are either sufficiently high or substantially low. However, materials that meet these requirements are chemically unstable, corrosive, or synthetically difficult to prepare.[1c]

Porous organic polymers (POPs) are a unique class of polymers that combine covalent π-networks with inherent porosity.[2] POPs are a class of emerging multifunctional materials and show outstanding properties and functions in various applications, such as gas storage,[3] light emitting,[4] energy transfer,[5] catalysis,[6] and energy storage.[7] They are highly stable as a result of a cross-linked network structure, and can be synthesized using a variety of different π-units. However, POP-based carrier-selective transporting materials remain to be explored.

Herein, we report the development of π-electronic POPs as a platform for designing electrode interlayers that feature robust chemical stability, tunable work function, and outstanding performance for energy conversions. We designed a basic structure, that is, BC (borane appended with carbazoles), which bears a tris(2,3,5,6-tetramethylphenyl) borane (TPB) focal core with three N-substituted carbazole groups at the periphery as electroactive units (Figure 1a; Supporting Information). The polyborane carbazole (PBC) films were prepared and fabricated through electropolymerization with concurrent polymer-film deposition, which has proven to be a useful method for the preparation of electroactive and conductive polymer films.[8] Upon electropolymerization, the N-substituted carbazole units form cation radical species that are highly active in coupling with each other, and form dimers with near-complete efficiency without the generation of other oligomers.[8] The resulting PBC thin films were formed on electrodes (ITO, Au, ZnO, and PEDOT:PSS) through multi-cycle cyclic voltammetry (CV) of the BC monomer (4.4×10^{-4} M) in a mixture of acetonitrile and dichloromethane (1:4 v/v) that contained tetrabutylammonium hexafluorophosphate (TBAPF$_6$) electrolyte in air at room temperature. During the positive CV scan, the onset oxidative potential was observed at 0.88 V, which was attributed to the oxidation of the carbazole,[8] whereas oxidation of the TPB unit was observed at 1.40 V (Supporting Information, Figure S1). During the negative scan, two reductive peaks were observed at 0.92 and 0.64 V, which were assigned to the reduction of the cations of TPB and dimeric carbazole, respectively. Consequently, we set up a potential range between −0.8 and 1.0 V for the film

[*] Dr. C. Gu,[+] N. Huang,[+] Prof. Dr. D. Jiang
Department of Materials Molecular Science
Institute for Molecular Science
National Institutes of Natural Sciences
5-1 Higashiyama, Myodaiji, Okazaki 444-8787 (Japan)
E-mail: jiang@ims.ac.jp

Y. Chen,[+] H. Zhang, S. Zhang, Prof. F. Li
State Key Laboratory of Supramolecular Structure and Materials
Jilin University
Changchun 130012 (P.R. China)

Prof. Y. Ma
State Key Laboratory of Luminescent Materials and Devices
Institute of Polymer Optoelectronic Materials and Devices
South China University of Technology
Guangzhou 510640 (P.R. China)

Prof. Dr. D. Jiang
Present address: Academic Field of Energy and Environment
School of Materials Science
Japan Advanced Institute of Science and Technology
1-1 Asahidai, Nomi 923-1292 (Japan)
E-mail: djiang@jaist.ac.jp

[+] These authors contributed equally to this work.

⊟ Supporting information for this article is available on the WWW under http://dx.doi.org/10.1002/anie.201510723.

a)

b) c)
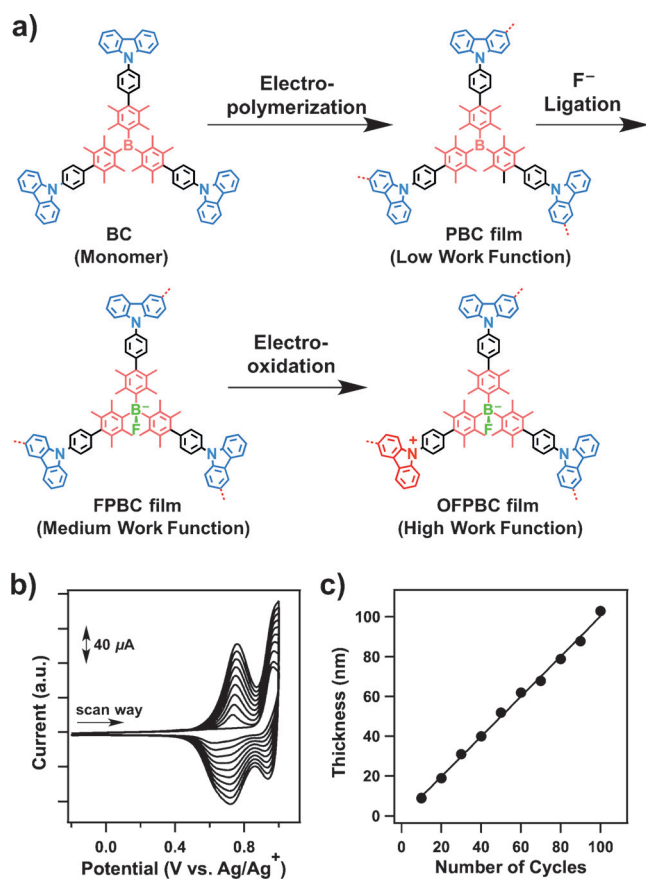
Figure 1. a) Representation of the design of monomer and preparation of POP films through electropolymerization. Polymerization of BC resulted in a low work function PBC film that possesses an extremely low HOMO level and serves as an electron-selective electrode. Upon F⁻ ligation to the boron atoms and electro-oxidation of the carbazole units, the resulting OFPBC films greatly raise the HOMO level and function as hole-selective electrodes. b) CV curves of BC recorded for 10 scan cycles (potential from −0.2 to 1.0 V). c) The thicknesses of the PBC films under different numbers of CV cycles (scan rate: 0.4 Vs⁻¹).

preparation. A positive potential in this range could only oxidize the carbazole units, whereas a sufficiently low negative potential ensured the complete reduction of the dimeric carbazole cations to neutral carbazoles and the removal of their counterions (PF_6^-) from the films.[8] From the second cycle in the continuous CV scan (Figure 1 b), a new oxidative peak appeared at 0.76 V, which is attributed to the oxidation of dimeric carbazoles.[8] The current increased as the cycle number increased, which suggests that more dimeric carbazoles formed and that the PBC films grew on the electrodes upon polymerization.

Infrared, electronic absorption, and X-ray photoelectron spectroscopy (XPS) revealed that the content of monomeric carbazole units in the films was negligible (Figures S2, S3a, and S4). One significant feature is that this electropolymerization-based synthetic method enables control over the film thickness. Indeed, a series of thin films were successfully synthesized by simply changing the cycle numbers. From the plot of film thickness versus CV cycle number, each CV cycle produced approximately 1 nm of film thickness at a scan rate

of 400 mV s⁻¹ (Figure 1 c). High-resolution transmission electron microscopy (HR-TEM) and Kr adsorption isotherm measurements confirmed that the films consisted of homogeneous porous networks (Figure S5), with a Brunauer–Emmett–Teller (BET) surface area of 1074 m² g⁻¹ and a pore size of 1.5 nm (Figure S6). Atomic force microscopy (AFM) measurements revealed that a 10-nm-thick PBC film uniformly covered the ITO surface and exhibited a smooth morphology over a large area, with a root-mean-square (RMS) roughness of only 0.85 nm (Figure S7). The roughness of the films remained constant, regardless of the film thickness and oxidative state (see below) of the films (Figure S7). The smooth film morphologies fully satisfy the requirements for optoelectronic devices.

The ligation of F⁻ ions to the borane units was conducted by immersing the PBC Films in THF solutions that contained various concentrations of (n-C_4H_9)$_4$NF, followed by multiple rinses with THF. The porous structure of the PBC film allowed for an easy access of fluorine ions to the boron atoms, and resulted in homogeneous ligation in the network. The XPS spectra of the resulting FPBC films revealed the disappearance of the B1s peak at a high binding energy of 189.4 eV and the appearance of a 185.5-eV peak at a low binding energy (Figure S8a), indicating the F⁻ coordination and the subsequent reduction in the electron-accepting ability of the FPBC films. The XPS spectra further revealed that the content of fluorinated borane units was precisely controlled by adjusting the concentration of F⁻ and the immersion time (Table S1). The fully fluorinated films were electro-oxidized to transform the dimeric carbazole units into their cations, which are known to be high work function moieties.[9] When a positive potential at 0.95 V was applied, the FPBC films were oxidized to yield dimeric carbazole cations and ClO_4^- counter ions. XPS measurements revealed that the contents of dimeric carbazole cations in the oxidized FPBC (OFPBC) films could be tuned by regulating the oxidative potential, whereas the fluorinated borate units remained unchanged (Figure S8b–d, Table S1). This solution-process procedure is widely applicable to different substrates, including ITO, Au, ZnO, and PEDOT:PSS. The F⁻ ion coordination and electro-oxidation significantly changed the absorption and emission properties of the films (Figure S3b,c).

To investigate the work functions of these POP films, we measured ultraviolet photoelectron spectroscopy (UPS) of 20 nm-thick PBC, FPBC, and OFPBC films deposited on different conducting electrodes. Figure 2a summarizes the UPS results. The PBC films possess an extremely low work function, whereas the fluorine-ligated FPBC and oxidized OFPBC films increase their work functions over a wide range to achieve a substantially higher work function.

ITO is a conducting substrate with a work function of 4.78 eV; this medium work function value renders it incapable of either electron- or hole-selective conduction. In optoelectronics, electrodes with selective electron and hole conductions are essential. When ITO was covered with a 20-nm-thick PBC film, a sufficiently low work function of 4.05 eV was achieved (Figure 2b). This low work function endows the electrode with selective electron transporting functions. Notably, the work function greatly increased to 4.48 and
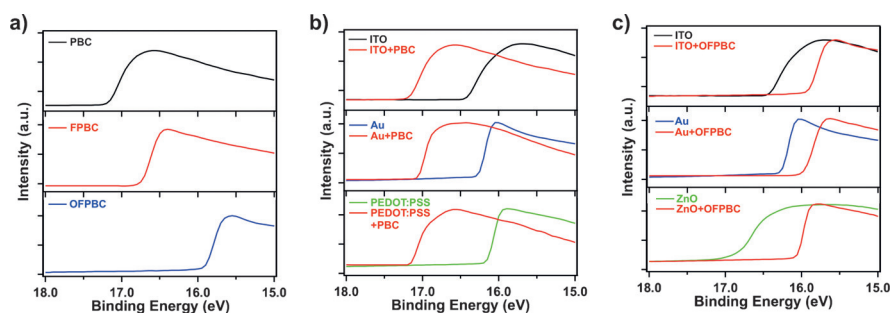
Figure 2. Secondary electron cut-off obtained by UPS for a) PBC, FPBC, and OFPBC films; b) ITO, Au, and PEDOT:PSS samples with and without 20 nm-thick PBC films; and c) ITO, Au, and ZnO samples with and without 20 nm-thick OFPBC films. The shift represents the change of the work function.

5.25 eV as the POP film was changed to FPBC and OFPBC, respectively (Figure S9). Indeed, the OFPBC film on ITO led to a work function that was high enough to serve as a hole-selective electrode (Figure 2c). We further investigated the effect of POP films on other typical conducting substrates, including Au, ZnO, and PEDOT:PSS. For this purpose, we prepared PBC, FPBC, and OFPBC films on these substrates, respectively. A 20 nm-thick PBC film on Au and PEDOT:PSS substantially decreased their work functions from 4.93 to 4.14 eV and from 5.05 to 4.05 eV, respectively (Figure 2b, Table S2). These decrements enabled their use for selective electron conduction. Therefore, the PBC films sufficiently reduced the work functions of the conducting substrates to yield low work function electrodes, which facilitate the injection or collection of electrons. In contrast, a 20 nm-thick OFPBC film increased the work functions from 4.93 to 5.23 eV for Au and from 4.33 to 5.11 eV for ZnO, respectively (Figure 2c, Table S2). These results clearly indicate that the OFPBC films serve as high work function interlayers that allow for injection or collection of holes in optoelectronic devices.

The thermal and air stabilities of PBC and OFPBC films on ITO substrates were studied by UPS measurements. The work functions of neither the PBC nor the OFPBC electrodes exhibited any change up to 200°C (Figure S10a). Both the PBC- and OFPBC-coated ITO electrodes were fairly stable under ambient conditions for more than 6 weeks; the work function variations were less than 0.3 eV (Figure S10b).

To investigate whether the thickness of the thin film affects the work functions, we prepared a variety of PBC and OFPBC films with different thicknesses ranging from 2 to 20 nm on ITO. The work function decreased to be lower than 4.1 eV when the PBC film was thicker than 15 nm, whereas the work function increased to be greater than 5.2 eV when the thickness of the OFPBC film was larger than 15 nm (Figure S10c). These observations demonstrated that the POP films with thicknesses of only 15 nm were sufficient to enable the selective flow of holes and electrons.

To investigate the performance of these high and low work function POPs, we fabricated energy-converting devices, including four different types of organic solar cells and light-emitting diodes using PBC and OFPBC on ITO as interlayers. We fabricated inverted organic solar cells (iOSCs)

and conventional organic solar cells (cOSCs) using PBC and OFPBC on ITO as anodes and cathodes, respectively. In both cells, poly(thieno[3,4-b]thiophene/benzodithiophene) (PTB7) and [6,6]-phenyl C_{71}-butyric acid methyl ester ($PC_{71}BM$) (1:1.5 by weight) were used as the photoactive layer.[10] In iOSCs, the MoO_3/Al functioned as anode; in cOSCs, LiF/Al acted as cathode. The device configurations of iOSCs and cOSCs were ITO/PBC film (15 nm)/PTB7:$PC_{71}BM$ (100 nm)/MoO_3 (10 nm)/Al (100 nm) and ITO/OFPBC film (10 nm)/PTB7:$PC_{71}BM$ (100 nm)/LiF (0.5 nm)/Al (100 nm), respectively (Figure 3a,d). We optimized the film thickness of PBC and OFPBC films and the dimeric carbazole cation content of the OFPBC films to yield the best device performance (Figures S11, S12). Figure 3b and e presents the *J*–*V* characteristics of the iOSC and cOSC in the dark and under illumination. The *J*–*V* characteristics in the dark reveal large rectification and a small reverse saturation current, which demonstrates the electron- and hole-selectivity of the PBC and OFPBC films, respectively. The iOSCs with PBC-coated ITO electrodes (Figure 3c) yielded a power-conversion efficiency (PCE) of 6.88% (open-circuit voltage (V_{OC}) = 0.750 V, short-circuit current density (J_{SC}) = 15.80 mA cm^{-2}, and fill factor (FF) = 0.581). These large V_{OC} and J_{SC} values are attributable to the following two factors: 1) the low work function of PBC films minimized the electron-collecting barrier in the iOSCs, and 2) the large surface area of the porous PBC films vastly improved the contact with the photoactive layer and minimized the contact resistance (Table S3). For comparison, we further fabricated iOSCs using traditional ZnO nanoparticles as cathode interlayer, while keeping otherwise same cell configurations. This control iOSC exhibited a PCE of 6.33% (Figure S13a). Clearly, the PBC films exhibited higher performance compared to conventional ZnO nanoparticle (6.88% vs. 6.33%).

On the other hand, the PCE of cOSC with OFPBC-coated ITO electrodes was as high as 7.93% (Figure 3f; V_{OC} = 0.775 V, J_{SC} = 16.12 mA cm^{-2}, and FF = 0.635). This large FF value also provided evidence of the good hole-selectivity of the OFPBC films. To date, the PTB7:$PC_{71}BM$-based cOSCs exhibit a PCE of 5–7%.[10] Our cOSCs give rise to the highest efficiency for cOSCs. We also prepared control cOSC by using PEDOT:PSS as the anode, while otherwise keeping the same cell configurations for comparison. The control cOSC exhibited a PCE of 7.23% (Figure S13b). These results again indicate that our films are superior to the conventional interlayer materials. To our knowledge, the PCEs of the devices are among the highest reported in solar cells with porous polymers as interlayers.[8a] Significantly, both V_{OC} and J_{SC} were enhanced by using the PBC and OFPBC films. This result reflects the improved charge-selectivity of these PBC and OFPBC films. Organic solar cells usually show a trade-off between V_{OC} and J_{SC};[1] our results suggest that the design of
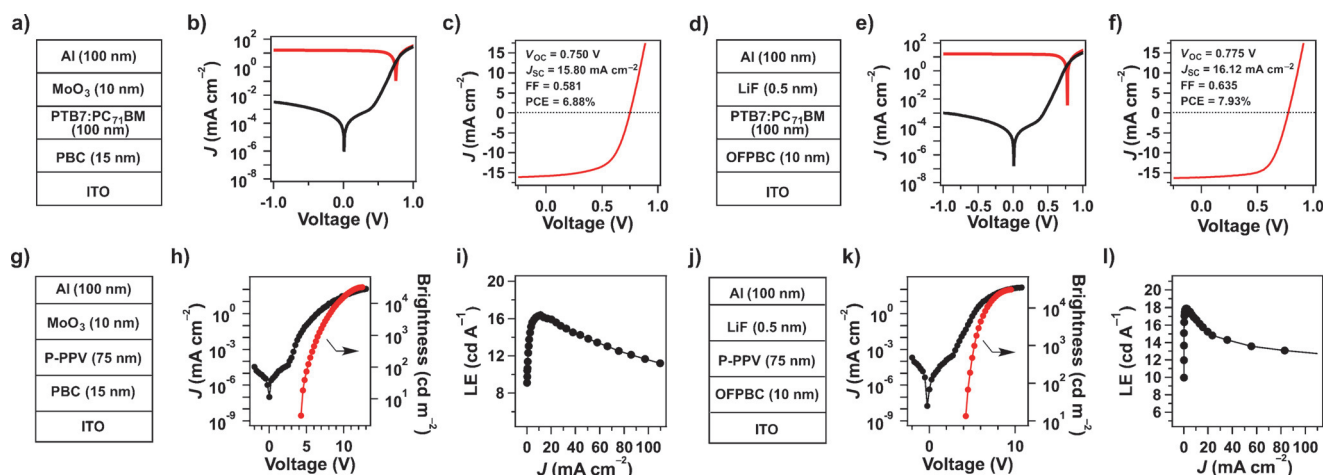
Figure 3. a) Device structure of the iOSCs based on the PBC film electrode. b) The J–V characteristics in the dark (black) and under illumination (red). c) J–V characteristics of the iOSCs under air mass (AM) 1.5 illumination (100 mW cm^{-2}). d) Device structure of the cOSCs based on the OFPBC film electrode. e) The J–V characteristics in the dark (black) and under illumination (red). f) J–V characteristics of the cOSCs under AM 1.5 illumination (100 mW cm^{-2}). g) Device structure of the iOLEDs based on PBC film electrode. h) Voltage-current-density-brightness characteristics of the iOLED. i) Current-density-luminous-efficiency characteristics of the iOLED. j) Device structure of the cOLEDs based on OFPBC film electrode. k) Voltage-current-density-brightness characteristics of the cOLED. l) Current-density-luminous-efficiency characteristics of the cOLED.

electrode interlayers may have a chance to break this limitation.

We investigated the performance of PBC and OFPBC films in organic light-emitting diodes (OLEDs). For this purpose, we fabricated inverted OLEDs (iOLEDs) and conventional OLEDs (cOLEDs) using an authentic green-emitting polymer, poly[2-(4-(3′,7′-dimethyloctyloxy)-phenyl)-*p*-phenylenevinylene] (P-PPV), as the light-emitting layer (Figure 3 g,j).[11] The iOLEDs had the configuration of ITO/PBC films (15 nm)/P-PPV (75 nm)/MoO$_3$ (10 nm)/Al (100 nm), whereas the cOLEDs had the configuration of ITO/OFPBC films (10 nm)/P-PPV (75 nm)/CsF (1.3 nm)/Al (100 nm). The PBC films on ITO in iOLEDs serve as the cathode, while the OFPBC films on ITO in cOLEDs function as the anode. Figure 3 h and k present the voltage-current-density-brightness characteristics of the optimal iOLEDs and cOLEDs, respectively (detailed data sets are summarized in Table S5). The two devices exhibited largely rectified J–V curves without any leakage current, and achieved maximum brightnesses of 30 000 (iOLED) and 32 500 cd m^{-2} (cOLED). Figure 3 i and l present the current-density-luminous-efficiency characteristics of the iOLEDs and cOLEDs, respectively. The two devices achieved maximum luminous efficiencies of 16.4 (iOLEDs) and 17.9 cd A^{-1} (cOLEDs). These values are among the best values reported for the green-emitting OLEDs.[11] In contrast, PEDOT:PSS-based cOLEDs (Figure S14, Table S5) exhibited a luminous efficiency of only 14.4 cd A^{-1}, indicating that the POP films are superior to conventional interlayers in producing high-efficiency OLEDs.

In summary, we have successfully designed a class of conducting materials capable of selective and efficient hole and electron flows based on porous organic polymers. The thin films offer an unprecedented example for electrode interlayers with robust chemical and thermal stabilities that are key to long-term performance. These thin films are compatible with various electrodes and offer outstanding

functions in various types of devices, including solar cells and light-emitting diodes. Our results reveal the enormous potential of porous organic polymers as an appealing platform for the rational design of work function, a newly developed aspect of POP materials worthy of further exploration. With the diversity of building blocks and tunability of POP structures, we envisage that POPs with different work functions would be useful not only in energy conversions but also in photocatalysis and energy storage.

[1] a) G. Yu, J. Gao, J. C. Hummelen, F. Wudl, A. J. Heeger, *Science* **1995**, *270*, 1789–1791; b) C. Duan, K. Zhang, C. Zhong, F. Huang, Y. Cao, *Chem. Soc. Rev.* **2013**, *42*, 9071–9104; c) Y. Zhou, C. Fuentes-Hernandez, J. Shim, J. Meyer, A. J. Giordano, H. Li, P. Winget, T. Papadopoulos, H. Cheun, J. Kim, M. Fenoll, A. Dindar, W. Haske, E. Najafabadi, T. M. Khan, H. Sojoudi, S. Barlow, S. Graham, J.-L. Brédas, S. R. Marder, A. Kahn, B. Kippelen, *Science* **2012**, *336*, 327–332.

[2] a) Y. Xu, S. Jin, H. Xu, A. Nagai, D. Jiang, *Chem. Soc. Rev.* **2013**, *42*, 8012–8031; b) A. G. Slater, A. I. Cooper, *Science* **2015**, DOI: 10.1126/science.aaa8075.

[3] a) Y.-C. Zhao, T. Wang, L.-M. Zhang, Y. Cui, B.-H. Han, *Polym. Chem.* **2015**, *6*, 748–753; b) Y. Luo, B. Li, W. Wang, K. Wu, B. Tan, *Adv. Mater.* **2012**, *24*, 5703–5707; c) X. Zhu, C. Tian, S. M.

Mahurin, S.-H. Chai, C. Wang, S. Brown, G. M. Veith, H. Luo, H. Liu, S. Dai, *J. Am. Chem. Soc.* **2012**, *134*, 10478–10484; d) S. A. Y. Zhang, Z. Li, H. Xia, M. Xue, X. Liu, Y. Mu, *Chem. Commun.* **2014**, *50*, 8495; e) Z.-Y. Sui, Y.-N. Meng, P.-W. Xiao, Z.-Q. Zhao, Z.-X. Wei, B.-H. Han, *ACS Appl. Mater. Interfaces* **2015**, *7*, 1431–1438.

[4] a) X. Liu, Y. Xu, D. Jiang, *J. Am. Chem. Soc.* **2012**, *134*, 8738–8741; b) Y. Xu, L. Chen, Z. Guo, A. Nagai, D. Jiang, *J. Am. Chem. Soc.* **2011**, *133*, 17622–17625.

[5] a) L. Chen, Y. Honsho, S. Seki, D. Jiang, *J. Am. Chem. Soc.* **2010**, *132*, 6742–6748; b) P. Zhang, K. Wu, J. Guo, C. Wang, *ACS Macro Lett.* **2014**, *3*, 1139–1144.

[6] a) L. Chen, Y. Yang, D. Jiang, *J. Am. Chem. Soc.* **2010**, *132*, 9138–9143; b) J.-X. Jiang, Y. Li, X. Wu, J. Xiao, D. J. Adams, A. I. Cooper, *Macromolecules* **2013**, *46*, 8779–8783; c) X. Ding, B.-H. Han, *Chem. Commun.* **2015**, *51*, 12783–12786; d) X. Ding, B.-H. Han, *Angew. Chem. Int. Ed.* **2015**, *54*, 6536–6539; *Angew. Chem.* **2015**, *127*, 6636–6639.

[7] a) F. Xu, X. Chen, Z. Tang, D. Wu, R. Fu, D. Jiang, *Chem. Commun.* **2014**, *50*, 4788–4790; b) Y. Kou, Y. Xu, Z. Guo, D. Jiang, *Angew. Chem. Int. Ed.* **2011**, *50*, 8753–8757; *Angew. Chem.* **2011**, *123*, 8912–8916; c) L. Wang, X. Feng, L. Ren, Q. Piao, J. Zhong, Y. Wang, H. Li, Y. Chen, B. Wang, *J. Am. Chem. Soc.* **2015**, *137*, 4920–4923.

[8] a) C. Gu, Y. Chen, Z. Zhang, S. Xue, S. Sun, K. Zhang, C. Zhong, H. Zhang, Y. Pan, Y. Lv, Y. Yang, F. Li, S. Zhang, F. Huang, Y. Ma, *Adv. Mater.* **2013**, *25*, 3443–3448; b) C. Gu, N. Huang, J. Gao, F. Xu, Y. Xu, D. Jiang, *Angew. Chem. Int. Ed.* **2014**, *53*, 4850–4855; *Angew. Chem.* **2014**, *126*, 4950–4955; c) C. Gu, N. Huang, Y. Wu, H. Xu, D. Jiang, *Angew. Chem. Int. Ed.* **2015**, *54*, 11540–11544; *Angew. Chem.* **2015**, *127*, 11702–11706; d) C. Gu, N. Huang, Y. Chen, L. Qin, H. Xu, S. Zhang, F. Li, Y. Ma, D. Jiang, *Angew. Chem. Int. Ed.* **2015**, *54*, 13594–13598; *Angew. Chem.* **2015**, *127*, 13798–13802; e) <> C. Gu, N. Huang, F. Xu, J. Gao, D. Jiang, *Sci. Rep.* **2015**, *5*, 8867; DOI: 10.1038/srep08867.

[9] A. Baba, K. Onishi, W. Knoll, R. C. Advincula, *J. Phys. Chem. B* **2004**, *108*, 18949–18955.

[10] a) M. Vasilopoulou, A. M. Douvas, L. C. Palilis, S. Kennou, P. Argitis, *J. Am. Chem. Soc.* **2015**, *137*, 6844–6856; b) R. Betancur, P. Romero-Gomez, A. Martinez-Otero, X. Elias, M. Maymó, J. Martorell, *Nat. Photonics* **2013**, *7*, 995–1000.

[11] a) H. Wu, F. Huang, Y. Mo, W. Yang, D. Wang, J. Peng, Y. Cao, *Adv. Mater.* **2004**, *16*, 1826–1830; b) W. Zeng, H. Wu, C. Zhang, F. Huang, J. Peng, W. Yang, Y. Cao, *Adv. Mater.* **2007**, *19*, 810–814; c) C. Zhong, S. Liu, F. Huang, H. Wu, Y. Cao, *Chem. Mater.* **2011**, *23*, 4870–4876.